Shrinking water's no man's land by lifting its low-temperature boundary

Markus Seidl,[1] Alice Fayter,[1] Josef N. Stern,[1] Gerhard Zifferer,[2] and Thomas Loerting[1,*]

[1]*Institute of Physical Chemistry, Universität Innsbruck, Innrain 80–82, 6020 Innsbruck, Austria*
[2]*Department of Physical Chemistry, Universität Wien, Währinger Straße 42, 1090 Wien, Austria*

Investigation of the properties and phase behavior of noncrystalline water is hampered by rapid crystallization in the so-called "no man's land." We here show that it is possible to shrink the no man's land by lifting its *low-temperature boundary*, i.e., the pressure-dependent crystallization temperature $T_x(p)$. In particular, we investigate two types of high-density amorphous ice (HDA) in the pressure range of 0.10–0.50 GPa and show that the commonly studied unannealed state, uHDA, is up to 11 K less stable against crystallization than a pressure-annealed state called eHDA. We interpret this finding based on our previously established microscopic picture of uHDA and eHDA, respectively [M. Seidl *et al.*, Phys. Rev. B **88**, 174105 (2013)]. In this picture the glassy uHDA matrix contains ice I_h-like nanocrystals, which simply grow upon heating uHDA at pressures ⩽0.20 GPa. By contrast, they experience a polymorphic phase transition followed by subsequent crystal growth at higher pressures. In comparison, upon heating purely glassy eHDA, ice nuclei of a critical size have to form in the first step of crystallization, resulting in a lifted $T_x(p)$. Accordingly, utilizing eHDA enables the study of amorphous ice at significantly higher temperatures at which we regard it to be in the ultraviscous liquid state. This will boost experiments aiming at investigating the proposed liquid-liquid phase transition.

I. INTRODUCTION

A lot of experimental and computational work has been devoted to the subject of distinct amorphous states of water since its discovery about 30 years ago [1,2]. Perhaps the most controversial discussions refer to the question whether or not these amorphous ices are glassy states being continuously connected to liquid phases at higher temperatures [3,4]. In principle, the amorphous ices, just like any disordered solid, may show unfreezing of rotational and/or translational degrees of freedom within the so-called glass transition range upon heating. If translation is involved, the amorphous solid softens and transforms to an ultraviscous liquid. Even though it is a matter of ongoing debate [5], such a behavior is rather well established for low-density amorphous ice (LDA) [6]. In comparison, studies on the glass transition of high-density amorphous ice (HDA) have been elusive for a longer time [6]. However, very recently, evidence for the transition of HDA to a corresponding high-density liquid was reported for both ambient [7] and elevated pressure [8–10]. That is, LDA and HDA appear to be glasses of two distinct liquid states, a finding that supports two-liquid theories of water. A first-order liquid-liquid transition has been recognized for some waterlike models [11–14] (for a recent review, see [15]), but its appearance is still highly disputed (see the most recent controversy on the extensively studied ST2 water model for an example [16–18]). However, it is striking that at temperatures above the hypothesized liquid-liquid critical point terminating the liquid-liquid transition line, two-state descriptions nicely reproduce the anomalous properties of water [19–21].

One reason for why the glass transition of HDA was elusive for more than two decades after its discovery in 1984 [1] is HDA's low thermal stability. HDA transforms to LDA upon heating at pressures <0.1 GPa [22,23], while it crystallizes at higher pressures [22–26]. Significant progress towards

detecting HDA's glass transition has been made by studying HDA annealed at elevated pressure [27–31]. HDA prepared via the original route [1] is called uHDA nowadays and relaxes towards a state called eHDA. Independent from details of the annealing treatment applied to relax uHDA [27,30,31], the resulting eHDA exhibits enhanced stability against transition to LDA at ambient pressure. As a consequence, the glass transition of eHDA at ambient pressure was identified utilizing two standard techniques for characterizing glasses: differential scanning calorimetry and dielectric relaxation spectroscopy [7]. Furthermore, also volumetric studies on eHDA at elevated pressure provide evidence for a glass transition in HDA [9]. From these studies it follows that eHDA rather than uHDA is the glassy counterpart of high-density liquid water.

Figure 1 depicts the "phase diagram" of the (stable and metastable) disordered forms of water for pressures 0.10–0.30 GPa, illustrating the metastability domains of supercooled liquid water and HDA. The two domains are separated by the so-called "no man's land" [3,32] (gray shaded area) in which bulk water crystallizes rapidly. Therefore, studies on the possible connection between pressurized supercooled water and amorphous ice are challenging. Coming from the high-temperature side (cf. Sec. 4 of the review by Caupin [33]), water freezes due to homogeneous nucleation at T_h upon cooling. Analogously, starting with eHDA (or uHDA) at the low-temperature side, the amorphous material crystallizes at T_x upon heating. We want to emphasize that both the homogeneous nucleation temperature T_h and the crystallization temperature T_x depend on the sample volume as well as on the experimental time scale, i.e., the cooling/heating rate applied in the respective experiment. For a constant volume, increasing the cooling (heating) rate results in a lower T_h (higher T_x). Therefore, studying the properties of liquid water (amorphous ice) at relatively low (high) temperatures requires very fast cooling (heating) and, of course, also very fast probing of small samples. Very recently, femtosecond x-ray laser pulses were

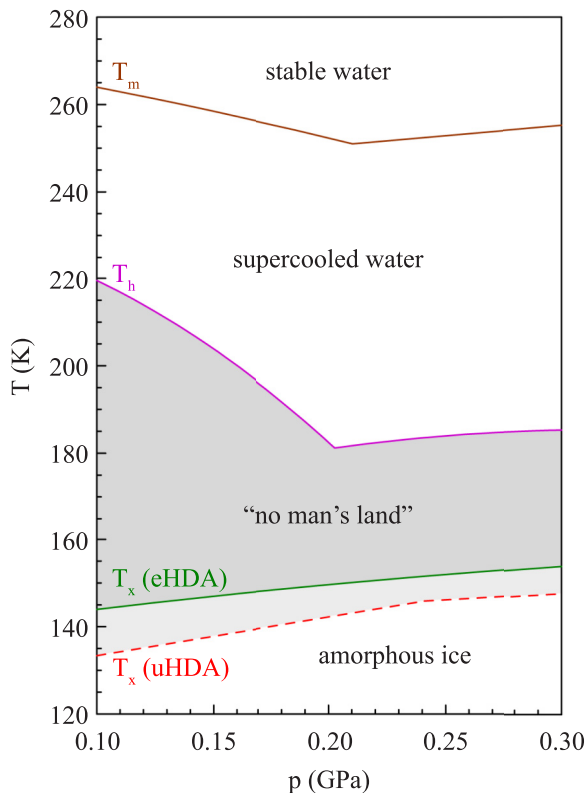*Corresponding author: thomas.loerting@uibk.ac.at

FIG. 1. (Color online) "Phase diagram" of disordered forms of water. T_m is the melting temperature and T_h is the homogeneous nucleation temperature. Both lines are redrawn from Fig. 6 in Ref. [4] and adapted originally from Ref. [80]. The T_h line is obtained upon isobaric cooling of emulsified liquid water droplets with ~3 K/min [80]. Lines denoted T_x are determined in the present study upon isobaric heating with 2 K/min (cf. Fig. 8) and represent the crystallization temperatures of two types of high-density amorphous ice (uHDA and eHDA, respectively). In the no man's land disordered forms of water crystallize extremely fast. If uHDA is considered (light-gray background), the no man's land is larger than in the case of eHDA (dark-gray background).
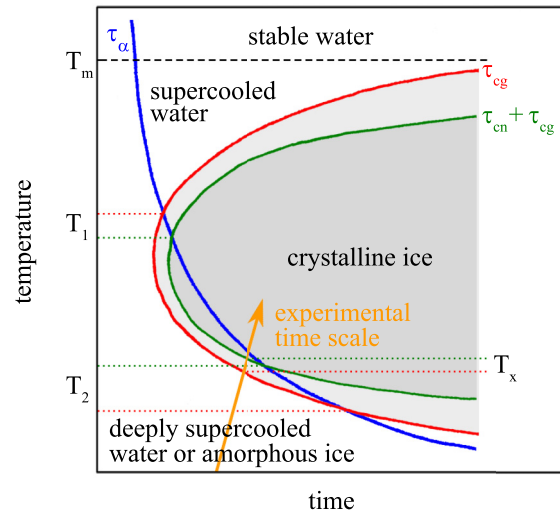

FIG. 2. (Color online) Proposed scenario for the relation between the time scales of structural relaxation and crystallization of water. The dashed line indicates the melting temperature T_m. τ_α is the structural relaxation time, τ_{cn} is the characteristic time of crystal nucleation, and τ_{cg} is the characteristic time of crystal growth. That is, the red curve marked τ_{cg} illustrates the crystallization time scale as observed in seeded samples (crystal growth only), while the green curve marked $\tau_{cn} + \tau_{cg}$ illustrates the crystallization time scale for initially completely noncrystalline samples (crystal nucleation followed by crystal growth). Both curves provide the characteristic time the system takes to form a certain amount (e.g., experimentally detectable fraction) of crystalline material. Each of the two crystallization curves intersects the blue relaxation curve at the temperatures T_1 and T_2. Thus, these temperatures represent the approximate limits between which water crystallizes faster than it relaxes. For times exceeding τ_{cg} (crystal growth only, light-gray background) or $\tau_{cn} + \tau_{cg}$ (crystal nucleation followed by crystal growth, dark-gray background), the sample contains at least a certain fraction of crystalline material. The orange arrow illustrates the time scale of the isobaric heating experiments (given by the heating rate of 2 K/min) reported in the present study. The crystallization temperature T_x obtained in these experiments is then given by the intersection of the arrow with the curve marked τ_{cg} (crystal growth only) or $\tau_{cn} + \tau_{cg}$ (crystal nucleation followed by crystal growth).

successfully used to probe the structure of micrometer-sized droplets of liquid water at subambient pressure down to a temperature of ~229 K [34]. Furthermore, studies on nanosized water droplets revealed T_h at a Laplace pressure of 0.05 GPa via Fourier-transform infrared spectroscopy [35]. Analogously, the temperature dependence of the heat capacity of doped [36] as well as pure [36,37] amorphous solid water was measured at ambient pressure utilizing ultrafast scanning calorimetry.

Experimental studies on noncrystalline water in the p-T region currently denoted no man's land are highly desired. In other words, it is required to shrink the no man's land by either pushing down the homogeneous nucleation limit T_h [34,35] or by lifting the crystallization temperature T_x. If successful, this will facilitate identification of the best of several theoretical scenarios aiming at an explanation of water's anomalous properties [4,38].

Within the last decade much computational work has been devoted to crystallization in water or waterlike models [39–43]. Such studies indicate that below a certain temperature, crystallization of the liquid might occur faster

than its equilibration [39,41,42]. That is, the time scales of crystallization (accounting for both crystal nucleation and subsequent crystal growth) and structural relaxation intersect at a certain temperature T_1 [44] (see Fig. 2 for a schematic illustration). Moreover, the time scales of crystallization and structural relaxation might intersect again at another temperature T_2 ($T_2 < T_1$) so that the noncrystalline state can be equilibrated above T_1 as well as below T_2. Such a scenario has been proposed theoretically by Kiselev and Ely [47]. Accordingly, they name the range between T_1 and T_2 "nonthermodynamic habitat." If the time scale of equilibration at $T \leqslant T_2$ is shorter than 100 s, then the system is regarded to be in the ultraviscous, deeply supercooled liquid state. The latter condition is, by definition [48], fulfilled above the glass transition temperature, $T > T_g$. In other words, at $T_g < T \leqslant T_2$ the ultraviscous liquid may be accessed experimentally. For low-density water such a scenario found strong experimental support [7], but also opposition [5]. In the case of high-density
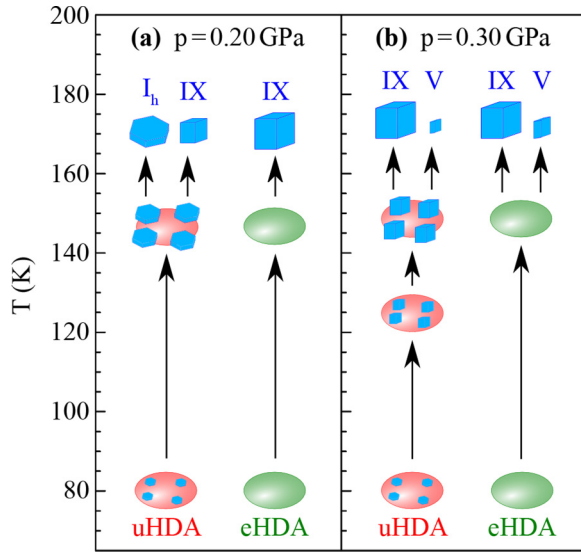
FIG. 3. (Color online) Sketch of the transformations taking place upon isobaric heating of starting materials uHDA (red) and eHDA (green) at 0.20 GPa (a) and 0.30 GPa (b), respectively. Amorphous material, i.e., HDA, is represented by ellipses. In uHDA nanocrystals of ice I_h are present (hexagonal prisms). These nanocrystals grow upon heating at pressures $\leqslant 0.20$ GPa (a), but upon heating at 0.30–0.50 GPa they first transform from ice I_h to ice IX nanocrystals (rhomboidal prisms) and start to grow subsequently (b). At pressures $\leqslant 0.20$ GPa uHDA transforms to a mixture of ice I and ice IX, while eHDA transforms to ice IX only (a). In contrast, at pressures 0.30–0.50 GPa a mixture of ice polymorphs (namely, ice IX and ice V) may be obtained from both uHDA and eHDA (b).

water its equilibration as an ultraviscous liquid seems to be possible, both at ambient pressure [7] and at elevated pressures up to ∼0.2 GPa [9,30] (for a review, see Ref. [6]).

Considering the outlined fundamental issues connected with water's no man's land, the exact locus of its low-temperature boundary for a wide pressure range, i.e., the crystallization line $T_x(p)$ of HDA, is highly interesting. While there are several studies on the crystallization of uHDA [22,24–26,49], the stability of eHDA against crystallization is less clear. Thus, we recently compared the crystallization behavior of uHDA with that of eHDA, considering the pressure range up to 0.20 GPa [23]. This study revealed two main observations [see Fig. 3(a) for 0.20 GPa]: (i) the higher crystallization temperature T_x in eHDA as compared to uHDA, and (ii) the change from growth of ice I plus a second polymorph from uHDA to crystallization of a single polymorph from eHDA. From these findings we have surmised that uHDA contains ice I_h-like nanocrystallites embedded in the HDA matrix, while eHDA obtained via high-pressure annealing [28,30] appears to be purely glassy [23]. However, bulk ice I_h, and thus presumably also the I_h-like nanocrystallites in uHDA, become less stable relative to other polymorphs upon increasing pressure (see the phase diagram in Fig. 4). Thus, it is of interest to study whether the phenomenology established at $\leqslant 0.20$ GPa in our earlier study [23] can also be observed outside the stability field of ice I_h at >0.20 GPa.

For this reason, we here report analogous crystallization studies on both uHDA and eHDA in the pressure range 0.30–0.50 GPa where bulk ice I_h is more stable than HDA
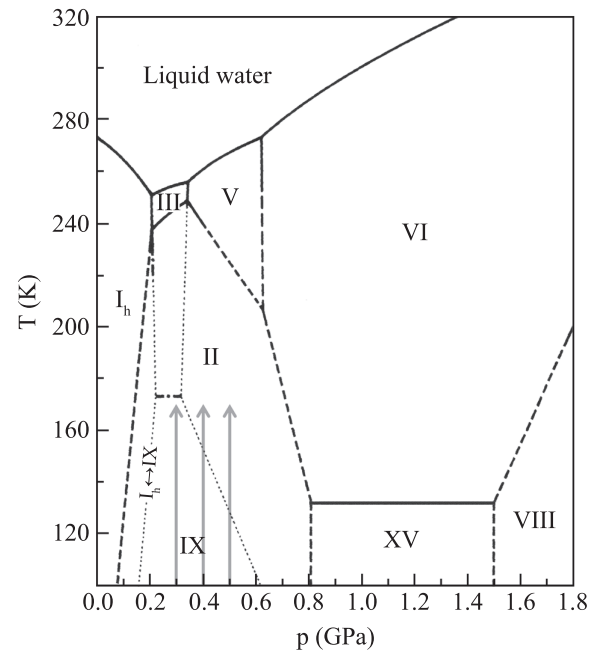

FIG. 4. Phase diagram of the stable phases of water, including metastable ice IX. Solid and dot-dashed lines indicate measured phase boundaries between stable and metastable phases, respectively. Dashed and dotted lines indicate extrapolated or estimated phase boundaries between stable and metastable phases, respectively. Gray arrows indicate the path of the isobaric heating experiments in the present study. Figure adapted from Ref. [81]; phase boundaries of ice XV as provided in Ref. [82].

but less stable than ice II (the most stable polymorph) and ice IX (a metastable polymorph) (cf. the extrapolated melting line of ice I_h provided by Mishima in Fig. 2(a) in Ref. [50]). The open questions to be addressed in this work are whether the ice I_h nanocrystals (i) grow at the expense of the HDA matrix, just like at $\leqslant 0.20$ GPa; (ii) first transform to ice II or ice IX nanocrystals which then grow at the expense of the HDA matrix; or (iii) whether they remain unaffected. If (iii) was the case, uHDA and eHDA would most probably show the same stability against crystallization and, moreover, crystallize to the same polymorphs. In contrast, if either (i) or (ii) was the case, eHDA would be more stable against crystallization than uHDA also at 0.30–0.50 GPa. In this paper we show that the ice I_h nanocrystals in uHDA indeed experience a phase transition to ice IX [see the illustration in Fig. 3(b)]. Therefore, for the whole pressure range of 0.10–0.50 GPa the low-temperature boundary of the no man's land is lifted by up to 11 K when considering eHDA instead of uHDA.

II. EXPERIMENT

A. Experimental setup

The experimental setup and protocol matched exactly the one applied in our previous study [23]. That is, both sample preparation and the crystallization studies themselves were conducted using a custom-made high-pressure piston cylinder setup (with a bore of 8 mm) as sample environment and a commercial "universal material testing machine" (Zwick, model BZ100/TL3S) for the application of pressure and measurement

of the piston displacement. The volume change ΔV of the samples was then calculated by multiplying the piston displacement with the area of the bore's cross section (assuming a temperature-independent bore diameter). Temperature was measured using a Pt-100 temperature sensor inserted firmly in the piston cylinder. While temperature was controlled utilizing a self-written LABVIEW program, pressure and sample volume were controlled using the software TESTXPERT 7.1 (Zwick). Further details on the apparatus are provided in Ref. [26].

B. Preparation of amorphous ices

uHDA was prepared from hexagonal ice I_h [1], which itself was produced by pipetting 300 μl liquid water into a precooled container made from thin indium foil with a mass of $\sim$0.3 g. The ice I_h sample was cooled to a temperature of $\sim$80 K and isothermally compressed to 1.60 GPa, applying a rate of 0.100 GPa/min, leading to formation of uHDA. Afterwards, the sample was decompressed at 0.100 GPa/min and $\sim$80 K to the desired pressure, at which ice crystallization was investigated. For the preparation of eHDA, uHDA formed as described above was decompressed at $\sim$80 K to 1.10 GPa, applying a rate of 0.100 GPa/min, heated isobarically at a rate of 2 K/min to 160 K, subsequently cooled back to 140 K at a rate of 2 K/min and then isothermally decompressed at a rate of 0.020 GPa/min to 0.20 GPa. Immediately after having reached this final pressure, the sample was quenched isobarically to $\sim$80 K and compressed at 0.020 GPa/min to the desired pressure.

C. Crystallization studies

In the crystallization studies, uHDA or eHDA was heated isobarically to a certain maximum temperature T_{max} at a rate of 2 K/min. In some experiments the sample was heated only once and quenched to $\sim$80 K upon reaching T_{max}. In the other experiments the sample was cooled slowly at $\sim$2 K/min from T_{max} to $\sim$115 K and then quenched to $\sim$80 K. Afterwards the sample was heated to T_{max} another one or two times. Upon reaching T_{max} in the last heating run, the sample

was quenched to $\sim$80 K directly and recovered at ambient pressure after release of pressure. In all experimental steps, the indium foil covering the ice sample acts as low-temperature lubrication medium, thus preventing sudden pressure changes and shock-wave heating associated with pressure drops [1,51]. All quench-recovered samples were characterized by x-ray powder diffraction (Cu $K\alpha_1$ radiation) in θ-θ geometry at $\sim$80 K and (sub)ambient pressure. The measurements were done using a diffractometer from Siemens (model D 5000) with a low-temperature camera from Anton Paar mounted onto it.

D. Analysis of volume curves

Figure 5 illustrates that the volume change $\Delta V(T)$ observed upon crystallization of HDA may be strongly positive, strongly negative, or anywhere in between, depending on heating rate and the starting material employed. The pressure-dependent densities $\rho(p)$ of uHDA, ice IX, and ice V are shown in Fig. 5(a). From their relation it follows that uHDA crystallizing to ice IX is associated with a volume increase as shown in the upper row of Fig. 5(b) for both slow (curve 1) and fast crystallization (curve 2). In contrast, uHDA crystallizing to ice V is associated with a volume decrease (curve 3). However, it has been shown that uHDA usually does not crystallize to a single ice phase but to a mixture of several ice polymorphs [25]. For example, isobaric heating in the pressure range 0.30–0.50 GPa may result in a mixture of ice IX, ice V, and ice I_h, where the respective phase fractions depend on the heating rate [25]. That is, upon heating HDA in this pressure range the volume change ΔV caused by crystallization can also be complex. Depending on which crystallization processes are actually taking place, the $\Delta V(T)$ curve may exhibit different shapes [see the schematic examples in the lower row of Fig. 5(b)].

E. Definition of crystallization temperatures

Where applicable, the onset point of crystallization is defined by the intersection of a straight line through the low-temperature part with a straight line through the midtemperature part of the $\Delta V(T)$ curve. Analogously, the
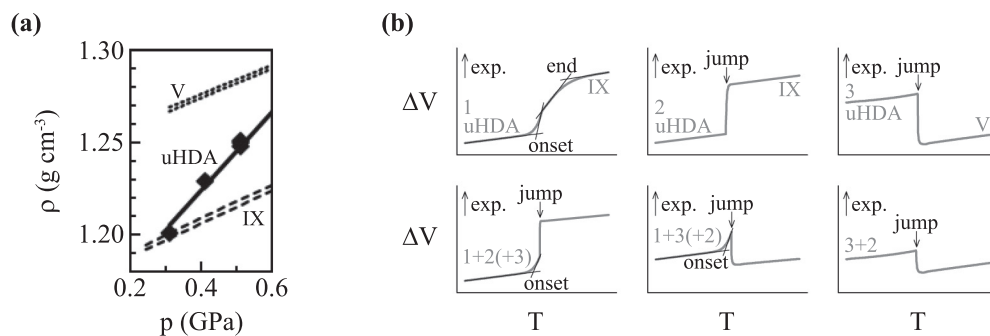

FIG. 5. Density or volume change associated with crystallization upon isobaric heating of HDA. Panel (a) provides the pressure-dependent density $\rho(p)$ of uHDA, ice IX, and ice V, respectively; the figure is a cut-out of Fig. 2 in Ref. [26] (adopted with changes). In panel (b) the evolution of volume change $\Delta V(T)$ upon crystallization of starting material uHDA is illustrated schematically. The arrow (labeled "exp.") close to the ordinate indicates the direction of expansion. The figures in the upper row show the volume increase upon slow (curve 1) and fast crystallization of ice IX (curve 2) as well as volume decrease upon fast crystallization of ice V (curve 3). The figures in the lower row illustrate a more complex crystallization behavior caused by parallel crystallization kinetics. Labels refer to the curves shown in the upper row and indicate the distinct crystallization processes taking place in one and the same sample. Straight lines illustrate how the onset and end point of crystallization are defined (for details see Sec. II in the main text).

end point of crystallization is defined by the intersection of a straight line through the high-temperature part with a straight line through the midtemperature part of the same curve. However, the midtemperature region is often found to be nonlinear, e.g., because of competing crystallization channels to the same ice phase [cf. curve 1 in Fig. 5(b)] or because of multiple ice phases crystallizing [cf. curves labeled "1+2(+3)" and "1+3(+2) in Fig. 5(b)]. If a sudden volume jump occurs, the onset point of crystallization is defined by the intersection of a straight line through the low-temperature part with a straight line through the data just prior to the sudden volume jump. Please note that in this case the onset temperature of crystallization represents a lower limit and refers to the crystallization temperature of the ice phase

crystallizing first at low temperatures. We refrain from the definition of a second onset temperature pertaining to the ice phase crystallizing at higher temperature, because this is affected by the extent to which the first phase has already consumed the amorphous matrix.

F. Reproducibility

In order to investigate the reproducibility of the experiments and to follow the temperature development of ice polymorph mixtures utilizing *ex situ* powder x-ray diffraction, we obtained an extensive set of data with different maximum temperatures T_{max} at 0.30 GPa. From the $\Delta V(T)$ curves presented in Figs. 6(a) and 6(b) it follows that the crystallization step
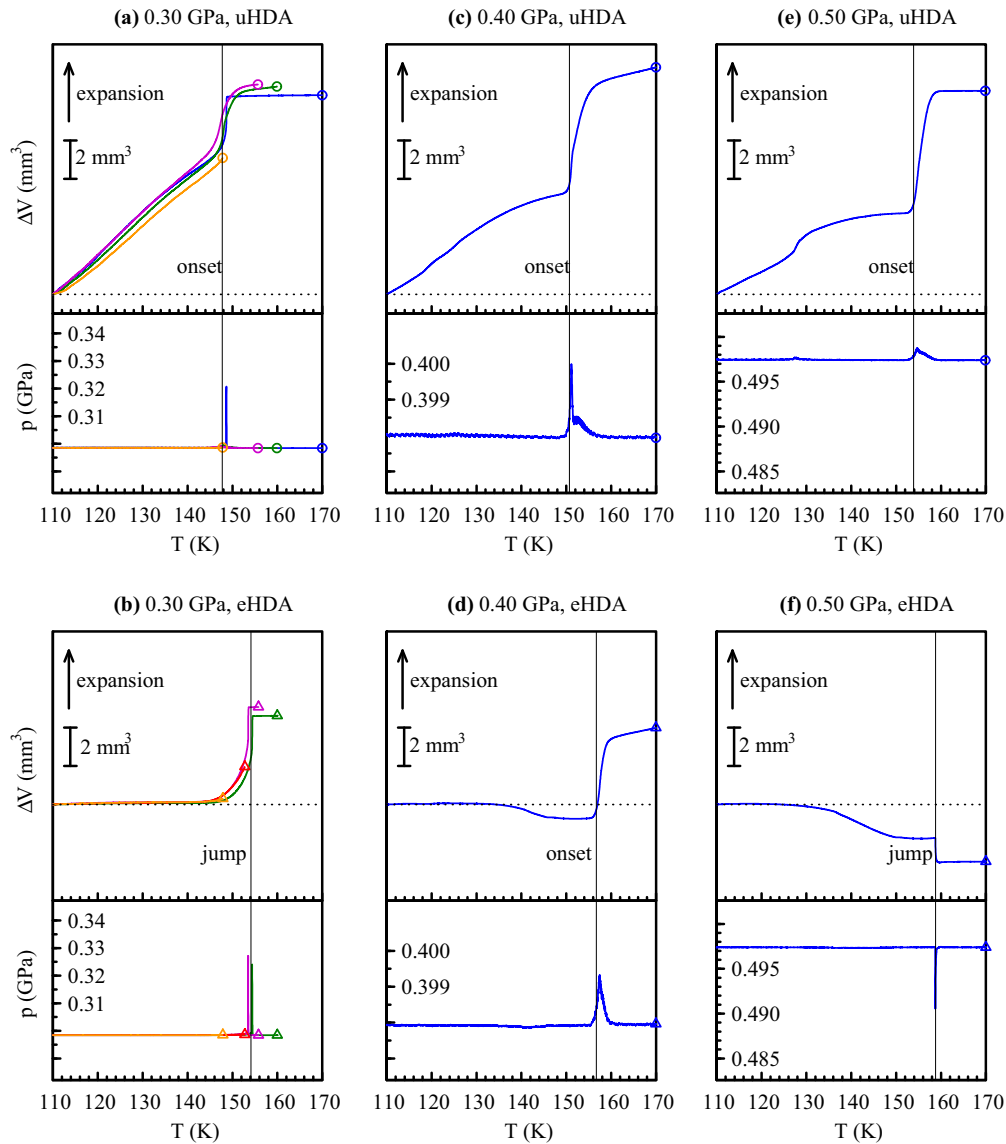

FIG. 6. (Color online) Volume change ΔV and pressure evolution while isobarically heating (2 K/min) high-density amorphous ices at 0.30, 0.40, and 0.50 GPa, respectively. Data for starting material uHDA are shown in the first row while data for starting material eHDA are shown in the second row. Colors refer to the maximum temperature T_{max} reached in the respective experiment; T_{max} is 148 K (orange), 153 K (red), 156 K (pink), 160 K (green), or 170 K (blue). Circles (uHDA) and triangles (eHDA) mark the end points of the curves at T_{max}. The $\Delta V(T)$ curves are corrected for the apparatus behavior (see Sec. II in the main text) and vertically shifted to match at 110 K. The dotted horizontal line helps one recognize the positive or negative slope of the $\Delta V(T)$ curves. In each panel the solid vertical line indicates the crystallization temperature T_x as plotted in Fig. 8(b), considering either the onset point or the position of the sudden volume jump.

is highly reproducible. In the $p(T)$ curves, which should in principle reflect the isobaric nature of the crystallization experiment, deviations from nominal pressure can be up to $\pm 13\%$. These are caused by rapid volume change upon fast crystallization.

G. Apparatus correction

Please note that the $\Delta V(T)$ curves reported here show the behavior of the ice samples only, while the ones in our previous study [23] included the contribution of the apparatus. This contribution comes mainly from the steel pistons which transmit the pressure from the material testing machine to the sample. Since the apparatus itself exhibits a nearly linear volume change upon isobaric heating, a linear function (for each of the pressures) accounts for it in good approximation. Thus, the $\Delta V(T)$ curves reported in Fig. 6 were obtained by subtracting a linear function (representing the apparatus' contribution) from the raw data. The subtracted linear functions thenselves were obtained from isobaric heating experiments analogous to those on the indium-covered ice samples. However, in this case only

~ 0.3 g indium, but no ice was put into the pressure cell. Such an experiment to be used as a correction for the expansivity of the apparatus without ice sample was done at 0.30 and 0.50 GPa. In both cases a linear function was determined by fitting the $\Delta V(T)$ data in the range 145–165 K. The apparatus function's slope for the case of 0.40 GPa was then determined from the slopes of the linear functions obtained for 0.30 and 0.50 GPa by linear interpolation.

III. RESULTS

Figure 6 shows the volume change $\Delta V(T)$ as well as the pressure evolution $p(T)$ while isobarically heating uHDA (first row) and eHDA (second row) at 0.30, 0.40, and 0.50 GPa, respectively. The x-ray diffraction patterns of all quench-recovered samples together with those of the respective starting material (uHDA and eHDA, respectively) are shown in Fig. 7. Amorphous materials are usually characterized by the position of the maximum of the first halo peak for which we find $\sim 30.1°$ in the case of uHDA and $\sim 31.4°$ in the case of eHDA, being in good agreement with previous reports [see, e.g., curve (1) in
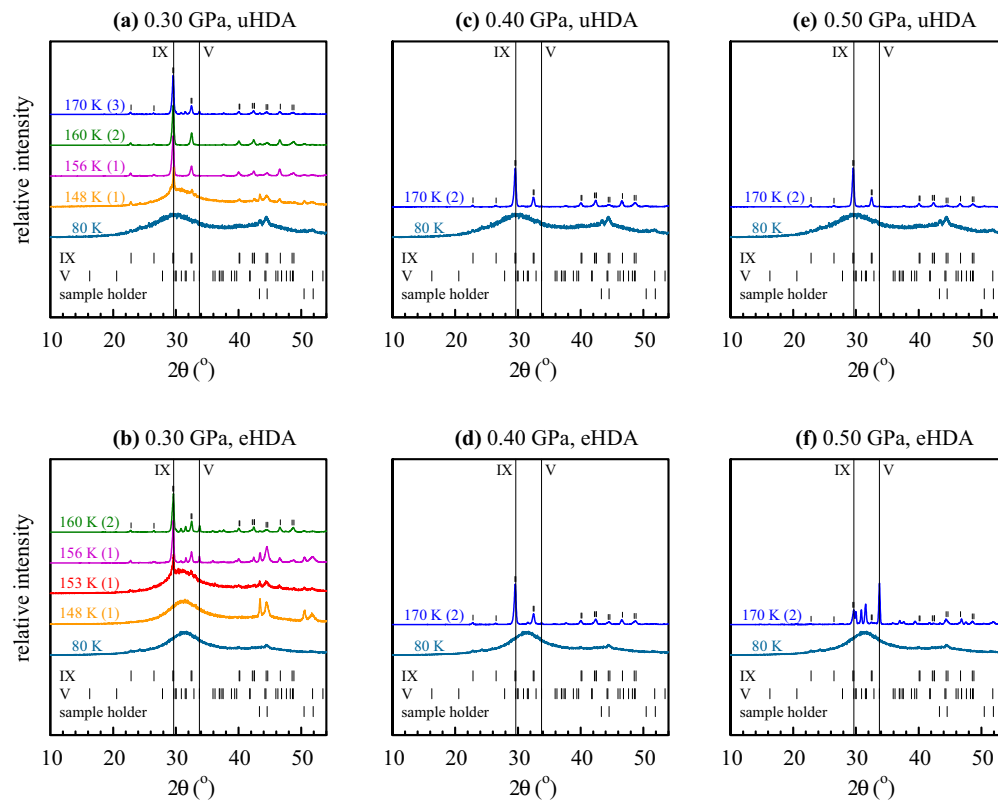

FIG. 7. (Color online) X-ray diffraction patterns of states obtained by isobaric heating of high-density amorphous ices at 0.30, 0.40, and 0.50 GPa, respectively (see Fig. 6), recorded after samples' recovery to ~ 80 K and (sub)ambient pressure. Curves are offset for clarity. Data for uHDA are shown in the first row while data for eHDA are shown in the second row. Temperature labels providing the maximum temperature reached in the respective experiment (as well as use of the same color code as in Fig. 6) allow assignment of the individual diffractograms to the samples' volumetric curves in Fig. 6. The number of heating/cooling cycles (for details, see Sec. II in the main text) are stated in brackets. In each panel the diffractogram labeled 80 K (turquoise curve) refers to the starting material, i.e., uHDA or eHDA. In the case of starting material uHDA (first row) the pattern shows a broad halo peak with a maximum at $\sim 30.1°$, while in the case of starting material eHDA (second row) the halo peak maximum occurs at $\sim 31.4°$. At the bottom of each set of diffractograms the Bragg peak positions of ice IX and ice V as well as those of the sample holder are indicated by tics (only peaks with a theoretical intensity of $> 2\%$ of the most intense peak's intensity are considered). The Bragg peak positions of ice IX are also marked in the diffraction pattern at the very top of each set. Vertical lines indicate the position of the most intense Bragg peak of ice IX and ice V, respectively. The intensities of the peaks found at these positions are used to estimate the phase composition of fully crystallized samples (see Table I).
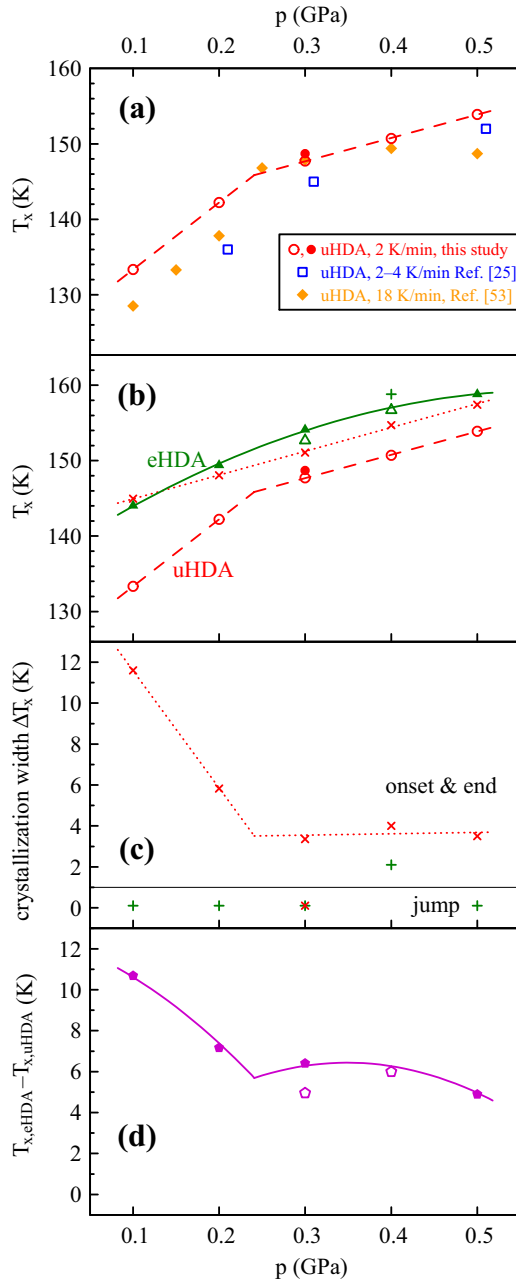
FIG. 8. (Color online) In panel (a) and panel (b) the crystallization temperature T_x of uHDA (circles) and eHDA (triangles), respectively, is plotted as a function of pressure. Open symbols correspond to the onset point of crystallization and full symbols to the sudden volume jump [cf. Fig. 5(b)]. The data are obtained from the $\Delta V(T)$ curves shown in Fig. 6 of the present paper, Figs. 2(d)–2(f) and Fig. SM3(d)–3(f) in Ref. [23], and similar curves of additional experiments (not shown). All data points at pressures 0.10–0.30 GPa represent mean values of two to five independent experiments, except the data point of uHDA obtained from a sudden volume jump at 0.30 GPa. This one as well as all data points at 0.40 and 0.50 GPa are based on only one experiment, where the respective $\Delta V(T)$ curve is shown in Fig. 6. The size of the symbols is equal to or larger than twice the standard deviation. In particular, panel (a) provides a comparison of our result for $T_x(p)$ of starting material uHDA with earlier results on the same material, while panel (b) provides a comparison of our result for both starting material uHDA and eHDA, respectively. Crosses and the plus correspond to the end

Fig. 6(a) in Ref. [26] for uHDA and curve marked "0.2 GPa" in Fig. 3(a) in Ref. [28] for eHDA].

The $\Delta V(T)$ curves in Fig. 6 exhibit several features caused by several distinct processes, namely, reversible thermal expansion, irreversible structural relaxation, and crystallization modes of the amorphous ice. Depending on the actual starting material (uHDA vs eHDA) as well as on the crystalline polymorph(s) actually crystallizing, both irreversible structural relaxation and crystallization are associated with a more or less pronounced volumetric feature as will be discussed in the following.

A. Reversible thermal expansion vs irreversible structural relaxation of HDA

We now analyze the $\Delta V(T)$ curves in Fig. 6 by following several temperature sequences, starting at the low-temperature end. For any material and any pressure (0.30–0.50 GPa) studied here, crystallization does not occur below $\sim$145 K (cf. Fig. 8 in Ref. [25] for uHDA) on the time scale given by the heating rate of 2 K/min. Thus, in addition to reversible thermal expansion only irreversible structural relaxation could affect $\Delta V(T)$. That is, the slope of any $\Delta V(T)$ curve below $\sim$145 K reflects reversible thermal expansion and, superimposed on it, eventually irreversible structural relaxation caused by the out-of-equilibrium nature of amorphous ices.

Being out of equilibrium is clearly the case for uHDA, which has been reported to be strained and far from equilibrium in the pressure range around 0.1–0.2 GPa [31]. Furthermore, upon heating uHDA at pressures below $\sim$0.5 GPa the halo maximum shifts to larger d spacings (i.e., smaller angles), indicating formation of an expanded HDA which is at most $\sim$2% less dense than uHDA [27]. As a consequence, significant irreversible structural relaxation associated with

---

FIG. 8. (*Continued*) point of crystallization of starting material uHDA and eHDA, respectively [cf. Fig. 5(b)]. The dashed lines are linear fits to the onset point of crystallization of starting material uHDA at pressures $\leqslant$0.20 GPa and 0.30–0.50 GPa, respectively. The dotted line is a linear fit to the end point of crystallization of starting material uHDA in the whole pressure range. The solid line is a quadratic fit to the temperature where a sudden volume jump occurred upon heating eHDA, again considering the whole pressure range. Panels (c) and panel (d) show the differences between several specific crystallization temperatures as a function of pressure. In panel (c), crosses and pluses depict the crystallization width ΔT_x for uHDA and eHDA, respectively. In both cases, a sudden volume jump has a pressure-independent width of $\sim$0.1 K (data points below the thin horizontal line). In experiments where no such volume jump occurred (data points above the horizontal line), the difference between the onset and end temperature of crystallization is at least $\sim$2 K; lines fitting the data of uHDA are analogously obtained from the respective fits plotted in panel (b). In panel (d), full pentagons depict the difference between the crystallization temperature of eHDA defined by the sudden volume jump and the crystallization temperature of uHDA as obtained from evaluation of the onset point; empty pentagons depict the difference between the crystallization temperature of eHDA and uHDA, respectively, both as obtained from evaluation of the onset point. The lines are analogously obtained from the respective fits plotted in panel (b).

volume expansion is expected upon heating uHDA at pressures below 0.5 GPa. In contrast, eHDA as prepared in the present study has been shown to be rather close to an equilibrated state under the conditions of its preparation, i.e., at 0.20 GPa and 140 K [30]. Our results reported here confirm these findings. First, the $\Delta V(T)$ curves obtained upon isobaric heating of starting material uHDA in the pressure range 0.30–0.50 GPa (Fig. 6, first row) show a much larger slope on the low-temperature side than those of eHDA (Fig. 6, second row), indicating pronounced structural relaxation associated with volume expansion taking place in uHDA. Second, the very flat nature of the $\Delta V(T)$ curves of eHDA at 0.30 GPa below 145 K [Fig. 6(b)] indicates the absence of irreversible structural relaxation, suggesting that eHDA is very close to equilibrium at 0.30 GPa. If this is indeed the case, eHDA is expected to show densification due to irreversible structural relaxation at higher pressures. In fact, densification is observed, being most pronounced in the temperature range 135–145 K at 0.40 GPa [Fig. 6(d)] and 125–150 K at 0.50 GPa [Fig. 6(f)]. The negative slope implies that the irreversible relaxation (causing densification) overcompensates the reversible thermal expansion by far. The finding of eHDA being very close to equilibrium at 0.30 GPa can be explained by considering its preparation. The final step in the preparation of eHDA is isothermal decompression from 1.10 GPa to 0.20 GPa at 140 K. In this step the initial very high-density state (existing at 1.10 GPa) [52] continuously transforms to less dense eHDA [28,30]. Because of finite transformation kinetics, the eHDA immediately quench recovered upon reaching 0.20 GPa is closest to equilibrium at a slightly higher pressure for which we find ∼0.30 GPa.

It should be noted that irreversible structural relaxation is typically most evident above 120 K, in both the case of starting material uHDA and the case of starting material eHDA. However, while starting material eHDA changes its behavior from thermal expansion to densification above ∼120 K, uHDA expands both above and below this temperature at any pressure considered here (0.30–0.50 GPa). Previous studies on the question of uHDA's expansivity in the same pressure range are ambiguous, giving support both for expansion [27] and compaction [26,53]. If the irreversible structural relaxation was complete, both types of HDA would show the same density. In fact, in an earlier study uHDA has been considered to be well relaxed just prior to crystallization in the pressure range 0.3–1.9 GPa [26], without providing explicit evidence. In general, our studies clearly support such a consideration for both uHDA and eHDA because the flattening of the $\Delta V(T)$ curves prior to crystallization indicates that irreversible relaxation no longer plays a role (Fig. 6). The only exception is uHDA at 0.30 GPa [Fig. 6(a)], which appears to be a still somewhat strained material at its crystallization temperature.

B. Crystallization of HDA

Above ∼145 K both types of HDA ultimately crystallize, where the associated density change leads to a steplike feature in the $\Delta V(T)$ curves [25,26]. The phase composition of such fully crystallized samples is summarized in Table I. As already discussed in Sec. II and illustrated in Fig. 5(b), there are several specific ways to define the crystallization temperature

TABLE I. Phase composition of fully crystallized samples. The data are estimates gained from x-ray diffraction patterns like those shown in Fig. 7 by calculating the quotient of the intensities of the most intense Bragg peaks of ice IX and ice V, respectively. Since the most intense ice IX Bragg peak is superposed with an ice V Bragg peak, the observed intensity had to be separated into two contributions. This was done by estimating the ice V Bragg peak's intensity from the observed intensity of the most intense ice V peak and the known intensity ratio of the two ice V Bragg peaks. In the case of 0.30 GPa the tabulated sample composition is derived from analysis of four to five independent samples, while at 0.40 and 0.50 GPa, respectively, only one sample has been studied. In all cases two diffraction patterns per sample were recorded, using material from different sample parts to account for a possible heterogeneity of the sample.

p (GPa)	Phase	uHDA	eHDA
0.30	IX	90%–100%	70%–95%
	V	0%–10%	5%–30%
0.40	IX	95%–100%	95%–100%
	V	0%–5%	0%–5%
0.50	IX	95%–100%	5%–40%
	V	0%–5%	60%–95%

on the basis of $\Delta V(T)$ curves. The onset temperature (end temperature) characterizes an early (late) stage of the crystallization, while the jump temperature locates the very sudden volume change due to very rapid crystallization. As far as applicable, we extracted all these characteristic crystallization temperatures T_x from the $\Delta V(T)$ curves presented here in Fig. 6 (0.30–0.50 GPa) as well as those shown in Figs. 2(d) and SM3(d) in Ref. [23] and its Supplemental Material (0.10 and 0.20 GPa). The resulting (mean) values of $T_x(p)$ are summarized in Fig. 8(b). Even though they will be discussed in detail in Sec. IV, we want to emphasize already here that for any pressure uHDA (circles) is less stable against crystallization than eHDA (triangles). Furthermore, uHDA usually crystallizes completely (crosses) before eHDA even starts to crystallize (triangles).

C. Ice V enhances crystallization kinetics of ice IX from HDA

At 0.30 GPa, the step in $\Delta V(T)$ indicating crystallization has a different shape in the case of starting material uHDA [Fig. 6(a)] compared to the case of eHDA [Fig. 6(b)]. The latter shows a very steep volume jump around 154 K, while the former lacks such a jump in two of three experiments. A spike in the pressure evolution $p(T)$ of the respective experiments [see the lower part of Figs. 6(a) and 6(b), respectively] reflects the sudden volume jump since the volume changes too fast for the automated material testing machine to keep the pressure constant. The *ex situ* x-ray powder diffraction patterns recorded for the quench-recovered samples allow us to explain these differences. Upon heating to a maximum temperature of ⩾156 K, both uHDA [Fig. 7(a)] and eHDA [Fig. 7(b)] crystallize completely. In the case of all experiments exhibiting a steep volume jump, the respective diffraction patterns identify the crystalline material to be a mixture of mainly ice IX and some ice V. In contrast, the two fully crystalline samples resulting from starting material uHDA

without any steep volume jump are pure ice IX. This suggests that the sudden volume jump is correlated with the presence of ice V. However, ice V crystallizing from HDA is associated with a volume *decrease* as illustrated in Fig. 5(b), curve 3. That is, the observed sudden volume *increase* must be due to very fast crystallization of ice IX [cf. curve 2 in Fig. 5(b)], where its extent is a bit reduced due to fast crystallization of the ice V found to be present, too. Therefore, it seems that the presence of ice V significantly enhances the crystallization kinetics of ice IX. The diffraction patterns characterizing the states obtained upon heating to lower temperatures [see Figs. 7(a) and 7(b)] indicate only HDA (eHDA: 148 K) and mixtures of HDA and ice IX (uHDA: 148 K; eHDA: 153 K), respectively. That is, the deviation from linear expansion behavior observed for temperatures below 148 K in the case of uHDA [Fig. 6(a)], and below 153 K in the case of eHDA [Fig. 6(b)], is due to the onset of ice IX crystallization. From this it follows that ice IX starts to crystallize at lower temperatures than ice V. Previous studies on the crystallization of HDA by Salzmann *et al.* [25] confirm this finding. In their work they discuss the crystallization behavior of starting material uHDA for a broad pressure range (0.2–1.9 GPa) as a function of heating rate. For all pressures studied, they find parallel crystallization kinetics of ice phases, where pressure determines the actual two polymorphs crystallizing (see Fig. 7 and Table I in Ref. [25]). Since crystallization rates are temperature dependent, a switchover from preferred ice IX to preferred ice V crystallization is observed upon heating at 0.30 GPa (cf. Fig. 9 in Ref. [25]). While we have found single crystallization kinetics for eHDA for pressures ⩽0.20 GPa [23], our present results for 0.30 GPa show parallel kinetics for both uHDA and eHDA.

D. Thermal stability of uHDA vs eHDA

The finding of higher thermal stability with respect to crystallization of eHDA compared to uHDA recently established at ⩽0.20 GPa [23] is also true at pressures ⩾0.30 GPa [see Fig. 8(b)]. Consequently, the kinetics of crystal nucleation and/or crystal growth are not the same for uHDA and eHDA also at, e.g., 0.30 GPa: While in the diffraction pattern of a sample heated to 148 K only amorphous material is evident in the case of starting material eHDA [Fig. 7(b)], the same temperature treatment leads to a mixture of HDA and ice IX in the case of starting material uHDA [Fig. 7(a)]. Furthermore, the diffraction patterns of eHDA heated to 153 K [Fig. 7(b)] and uHDA heated to 148 K [Fig. 7(a)] are highly similar and indicate the same phase composition. Thus, the onset temperature of ice IX crystallization is ∼5 K higher in eHDA than in uHDA. The $\Delta V(T)$ curves of the respective experiments reflect the different onset temperatures for crystallization of starting materials uHDA and eHDA, too. Heating uHDA leads to a significant deviation from linear expansion behavior a bit below 148 K [see Fig. 6(a)], whereas hardly any deviation from linearity is observed for starting material eHDA at the same temperature [see Fig. 6(b)]. Figure 8(b) summarizes the crystallization temperatures derived from the $\Delta V(T)$ curves and shows that in the case of 0.30 GPa—considering either the onset of slow crystallization (open symbols) or the jump due to fast crystallization of ice IX (full symbols)—a

difference of ∼5 K between the crystallization temperature of uHDA and eHDA, respectively, is obtained. Since the same quantitative result is found in the analysis of the diffraction patterns presented above, the suitability of $\Delta V(T)$ curves for evaluating onset crystallization temperatures is proven for pressures ⩾0.30 GPa. Whether uHDA crystallizes at 0.30 GPa to a mixture of ices IX and V or to pure ice IX only [see Fig. 7(a)] could be due to small differences in the starting material beyond our control.

Our results for crystallization upon heating at 0.50 GPa are fully consistent with those at 0.30 GPa. Again, upon full crystallization both starting material uHDA [Fig. 7(e)] and starting material eHDA [Fig. 7(f)] transform to a mixture of ice IX and ice V with a much larger relative amount of ice V in the case of eHDA (see also Table I). In the case of starting material uHDA only traces of ice V are found presumably because HDA has crystallized nearly completely to ice IX prior to reaching the temperature regime where ice V forms preferentially. Salzmann *et al.* also found a minor fraction of ice V when heating uHDA at 0.50 GPa with a somewhat smaller rate of ∼0.5 K/min; however, heating with a somewhat larger rate of ∼3.5 K/min resulted in mainly ice V [25]. Upon heating uHDA with rates ⩽2 K/min no sudden jump in the corresponding $\Delta V(T)$ curve consistently occurs in the study of Salzmann *et al.* [see Fig. 2(a) in Ref. [25]] and the experiment shown in Fig. 6(e).

In the case of heating starting material eHDA at 0.50 GPa, the $\Delta V(T)$ curve exhibits a jump due to sudden volume compaction [see Fig. 6(f)]. The corresponding diffraction pattern [Fig. 7(f)] shows that the main fraction is ice V, while the minor fraction is ice IX (see also Table I). This crystallization phenomenology is represented by the curve labeled "3+2" in Fig. 5(b) which schematically reflects very fast, simultaneous crystallization of ice V and ice IX. Hence, the volume jump is due to superposition of the volume effect caused by ice V formation (i.e., sudden compaction) and the one caused by ice IX formation (i.e., sudden expansion). The former overcompensates the latter, being in accord with the density relations shown in Fig. 5(a) and the observed phase composition. In comparison to uHDA, starting material eHDA is stable against crystallization up to a higher temperature also at 0.50 GPa. As a consequence, in the temperature range of preferred ice V formation a large fraction of amorphous material is still present in the case of eHDA, but not in the case of uHDA, explaining the quantitative difference in the phase composition of completely crystallized samples.

The data obtained at 0.40 GPa are consistent with the findings mentioned above and the hypotheses deduced from them. Ice IX is the main crystallization product both from uHDA [Fig. 7(c)] and eHDA [Fig. 7(d)] (see also Table I). The onset of crystallization is higher by ∼6 K for eHDA as compared with uHDA [Fig. 8(d)]. The $\Delta V(T)$ curve obtained upon isobaric heating of uHDA at 0.40 GPa [Fig. 6(c)] shows the same shape as that obtained upon heating of the same starting material at 0.50 GPa [Fig. 6(e)]. In both cases the volume expansion to the right of the vertical line marking the crystallization onset reflects the formation of ice IX. As in the case of starting material uHDA, a jumplike crystallization is absent also in the case of starting material eHDA being heated at 0.40 GPa [Fig. 6(d)]. We suppose that the absence of a sudden volume
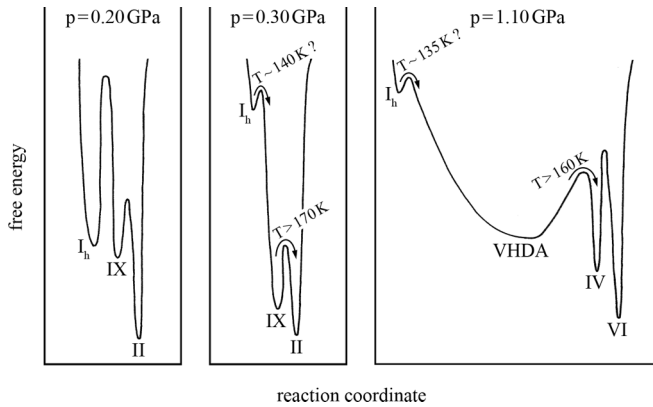
FIG. 9. Simplified schematic representation of the changes in the free energy surface upon changing pressure. The order of stability of crystalline and amorphous phases reflects experimental findings for bulk ices. Temperature labels indicate transition temperatures for *bulk* ices (IX → II and VHDA → IV) or *nanocrystalline* ices embedded in a HDA matrix (I_h → IX and I_h → VHDA). In each panel, crystalline and amorphous polymorphs that are irrelevant for the present discussion are omitted for clarity.

jump generally indicates almost complete consumption of HDA through ice IX crystallization prior to the onset of ice V crystallization. This is supported by the finding of just tiny amounts of ice V [see Figs. 7(c) and 7(d) and Table I].

IV. DISCUSSION AND CONCLUSIONS

In the Introduction we have motivated the present study by our recent suggestion of ice I_h-like nanocrystallites being present in uHDA, but not in eHDA [23]. These nanocrystallites explain why hexagonal ice I_h crystallizes upon isobaric heating of starting material uHDA at pressures up to 0.20 GPa, even though cubic ice I_c and/or ice IX usually grow from high-pressure ices at such conditions. eHDA, on the other hand, indeed shows growth of ice I_c and/or ice IX [see Fig. 3(a)]. The I_h-like nanocrystallites in uHDA just grow at the expense of the amorphous matrix upon heating at these low pressures.

We here focus our attention to the question how ice I_h-like nanocrystallites affect the crystallization phenomenology at higher pressures. At 0.30–0.50 GPa bulk ice I_h is significantly less stable than the high-pressure polymorphs ice IX, ice II, and ice V (cf. the phase diagram in Fig. 4 and the schematic free energy surface in the middle panel of Fig. 9). Therefore, upon isobaric heating of uHDA in this pressure region the nanocrystals could undergo a phase transition from ice I_h to ice IX or ice II before they actually start to grow at the expense of the HDA matrix [see Fig. 3(b)]. Due to the polymorphic phase transition of these nanocrystallites, the crystallization behavior observed at higher pressures would then be expected to deviate from that observed at lower pressures (where the I_h-like nanocrystals do not undergo a phase transition).

The results presented here indicate that in uHDA a polymorphic phase transition of the nanocrystals indeed takes place (similar to the crystal-crystal transformations in bulk ice [54–66]). Furthermore, they reveal that eHDA is not only more stable against crystallization than uHDA upon isobaric heating at ⩽0.20 GPa [23], but also at 0.30–0.50 GPa.

A. Stability against crystallization

Let us first compare our results for the onset crystallization temperature of starting material uHDA as obtained upon heating with 2 K/min (open circles) with literature [Fig. 8(a)]. Salzmann *et al.* obtained slightly smaller values (open squares) even though a similar heating rate of 2–4 K/min has been applied [25]. However, this deviation could be due to small differences in the definition of the onset of crystallization. Suzuki *et al.* obtained a sudden volume jump for heating uHDA at any pressure, corresponding to the rather high heating rate of 18 K/min applied in their study [53]. Accordingly, they evaluate the position of the jump as crystallization temperature. Since we obtain a similar shape of the $\Delta V(T)$ curve in one experiment on uHDA at 0.30 GPa, we can also compare their data (full diamond) to our own (full circle) [see again Fig. 8(a)]. In principle, the crystallization temperature is expected to increase with an increase in heating rate. That is, the crystallization temperatures reported by Suzuki *et al.*, which have been obtained upon heating with 18 K/min, are expected to lie above ours obtained upon heating with 2 K/min, which is clearly not the case. We speculate that minor experimental differences (e.g., details in temperature measurement) between their and our experiments are responsible for this deviation.

However, when considering all data shown in Fig. 8(a) it can clearly be recognized that all three independent studies agree in the remarkable feature that the pressure dependence of the crystallization temperature shows a linear regime below ∼0.25 GPa and another one with a smaller slope above this pressure. Interestingly, we previously found that a major fraction of ice I_h crystallizes from starting material uHDA up to 0.20 GPa [23], while this polymorph does not crystallize from the same material at pressures ⩾0.30 GPa [see Fig. 7 (first row) and Table I]. That is, the switchover in the onset crystallization temperature between two linear regimes at ∼0.25 GPa correlates with the presence or absence of ice I_h. We note that Salzmann *et al.* still find about 10% ice I_h at 0.31 GPa [25]. Nevertheless, a slightly higher pressure for the switchover of two linear regimes is in agreement with their data (see Fig. 8 in Ref. [25]). In remarkable contrast, upon isobaric heating of eHDA, a single (quadratic) curve fits the crystallization temperature in the whole pressure range [see the solid line in Fig. 8(b)]. The finding that no hexagonal ice I_h but cubic ice I_c crystallizes from eHDA at the low-pressure end [23] again supports the interpretation of ice I_h growth being at the bottom of the steep low-pressure crystallization line of starting material uHDA.

At all pressures from 0.10 GPa [23] to 0.50 GPa (Fig. 7), ice IX crystallizes from starting material uHDA parallel to ice I_h (0.10–0.20 GPa) and ice V (0.30–0.50 GPa), respectively. We have shown before that at 0.10–0.20 GPa ice I_h crystallizes first, i.e., at lower temperatures, while ice IX preferentially forms at higher temperatures [23]. Thus, the end point temperature of crystallization (crosses) [see Fig. 8(b)] has to be correlated with the formation of ice IX. This assignment seems to be true also at 0.30–0.50 GPa, even though ice V preferentially forms at higher temperatures in this case, because (if at all) only traces of ice V form from uHDA [see Fig. 7 (first row) and Table I]. In fact, the single linear function

fitting the end point temperature of crystallization [dotted line in Fig. 8(b)] supports this assignment. Accordingly, the crystallization width ΔT_x (as obtained by subtracting the end temperature from the onset temperature of crystallization) of starting material uHDA again reflects the two linear regimes of the onset temperature of crystallization [see the dotted line in Fig. 8(c)]. We conclude that the formation of ice I_h at pressures up to 0.20 GPa causes the large crystallization width, while for higher pressures where ice I_h is absent (0.30–0.50 GPa) a much smaller and pressure-independent width is obtained. The negative slope of the low-pressure linear regime of $\Delta T_x(p)$ can be explained by apparently decreasing kinetics of ice I_h formation with increasing pressure, leading to an increase of the crystallization's onset temperature. It is reasonable that the onset temperature of ice I_h crystallization increases with increasing pressure. Since ice I_h as low-density phase becomes less stable with increasing pressure, the driving force of the crystallization process determining its kinetics decreases too. For example, at 0.20 GPa ice I_h is metastable with respect to both ice IX and ice II, and thus, clearly less stable than below $\sim$0.10 GPa where it is the most stable form of ice (see the phase diagram in Fig. 4).

The crystallization width is in general much smaller for eHDA than for uHDA [see Fig. 8(c)]. eHDA (pluses) typically shows jumplike crystallization, whereas uHDA (crosses) crystallizes in a broader temperature interval. There is one exception in which the crystallization width for eHDA is $>$1 K and one exception in which the crystallization width for uHDA is $<$1 K [see the horizontal line in Fig. 8(c)].

Clearly, starting material eHDA [solid line in Fig. 8(b)] is much more stable against crystallization than starting material uHDA (dashed line). To quantify this finding we show the difference between the crystallization temperatures of the two distinct materials in Fig. 8(d). The stability difference between uHDA and eHDA drops from $\sim$11 K at 0.10 GPa to approximately 5–6 K at 0.30 GPa, above which a rather small pressure dependence is observed. The pronounced decrease of the relative stability of eHDA as compared to uHDA up to $\sim$0.30 GPa again reflects the formation of ice I_h which becomes less pronounced with increasing pressure and finally disappears between 0.20 and 0.30 GPa.

B. Crystal nucleation and crystal growth

We have mentioned before that both the actual locus of the crystallization line $T_x(p)$ and that of the homogeneous nucleation line $T_h(p)$ depend on the experimental time scale. However, we have shown above [Fig. 8(b)] that on one and the same experimental time scale the locus of $T_x(p)$ differs for uHDA and eHDA, i.e., for HDA prepared via different routes. This means that the size of water's no man's land is significantly smaller if eHDA rather than uHDA is studied (see Fig. 1). Since the experimental time scale does not differ in the present studies on uHDA and eHDA, the time scales of the respective crystallization processes have to be different in the two materials, as schematically indicated in Fig. 2.

Since we make use of powder x-ray diffraction here, it is reasonable to define the crystallization time scale as the time the system needs to form crystallites being large enough to be detected with standard powder diffraction techniques.

However, since we are running isobaric heating experiments instead of isobaric-isothermal (time-resolved) experiments, we may consider the temperature as a measure for the crystallization time scale. The crystallization time scale of either uHDA or eHDA would then be given by the temperature at which sharp Bragg reflexes due to crystalline material become visible in the diffraction pattern. Since we record *ex situ* diffraction patterns of quench-recovered samples (see Sec. II), we only probe the structure at certain maximum temperatures for the case of isobaric heating at 0.30 GPa. To rationalize the relation between the crystallization time scales of uHDA and eHDA we therefore compare them on the basis of diffraction patterns exhibiting approximately the same fraction of crystalline ice. As discussed in detail in Sec. III, isobaric heating of eHDA at 0.30 GPa to a maximum temperature of 153 K leads to a similar fraction of crystalline ice as heating uHDA to 148 K only. That is, the crystallization temperatures differ by $\sim$5 K, with eHDA being more stable against crystallization than uHDA. The crystallization time scales can now be drawn at least schematically (see Fig. 2) where the red curve (marked τ_{cg}) represents the case of uHDA, while the green curve (marked $\tau_{cn} + \tau_{cg}$) represent the case of eHDA.

From a comparison of the crystallization phenomenology exhibited by uHDA with that of eHDA at pressures up to 0.20 GPa, we have derived a microscopic picture of both types of HDA. We found strong evidence that uHDA contains ice I_h-like nanocrystallites embedded in the HDA matrix, while eHDA appears to be purely glassy [23]. As illustrated in Fig. 3(a), the nanocrystals present in uHDA simply grow upon isobaric heating at pressures $\leqslant$0.20 GPa. In contrast, in eHDA crystals first have to nucleate, resulting in a higher crystallization temperature as compared to uHDA. The crystallization time scales shown in Fig. 2 illustrate this scenario, too. Once a certain temperature is reached upon heating with a constant rate (orange arrow), the nanocrystals present in uHDA are able to grow, and thus they finally become detectable at T_x. In this case the crystallization temperature is given by the time scale of crystal growth τ_{cg} (red curve). In contrast, the crystallization temperature of eHDA is determined by the time scale of crystal nucleation and crystal growth, $\tau_{cn} + \tau_{cg}$ (green curve), resulting in a higher T_x. Both crystallization time scales cross the time scale of structural relaxation at individual temperatures T_2, above which HDA crystallizes faster than it relaxes. Upon heating either uHDA or eHDA at 0.20 GPa and a rate of 2 K/min (orange arrow), crystallization starts prior to reaching an equilibrated state, i.e., the liquid phase [67]. However, we have shown previously that eHDA can be equilibrated at pressures up to $\sim$0.2 GPa by subjecting the sample to consecutive heating/cooling cycles in which the maximum temperature lies below T_x [9]. Therefore, we have claimed that eHDA being metastable at low temperatures is indeed connected to a metastable liquid state at higher temperatures [6].

C. Polymorphic phase transition on the nanometer-length scale

The crystallization time scales illustrated in Fig. 2 depict the proper relation between the crystallization behavior of uHDA and eHDA for the whole pressure range from 0.10 to 0.50 GPa. However, the results of the present study in the pressure

range 0.30–0.50 GPa indicate that the nanocrystals affect the crystallization behavior of uHDA in a different manner to that of 0.10–0.20 GPa. While starting material eHDA is more stable against crystallization than starting material uHDA for pressures from 0.10 to 0.50 GPa, the phases obtained upon full crystallization differ between the two types of HDA up to 0.20 GPa, but not at higher pressures. The additional crystallization channel to ice I_h being active in uHDA due to the I_h-like nanocrystals disappears above 0.30 GPa, thus erasing the difference in uHDA and eHDA with respect to the obtained phases. However, the nanocrystals present in uHDA are still capable of accounting for its lower crystallization temperature as compared to eHDA. As mentioned in the beginning of the discussion, the nanocrystals could transform from ice I_h to ice IX upon heating at 0.30–0.50 GPa [see Fig. 3(b)], analogous to what is found for bulk ice I_h (see Fig. 1 in Ref. [65]). That is, it appears that such a polymorphic phase transition of the nanocrystals indeed takes place upon isobaric heating, provided the pressure is high enough. In the case of 0.30 GPa this phase transition takes place below 148 K because a sample having been heated to this temperature already contains some amount of ice IX [see Fig. 7(a)]. However, the difference between the crystallization temperature of eHDA and uHDA in the pressure range from 0.30 to 0.50 GPa is significantly smaller than below ∼0.2 GPa [see Fig. 8(d)]. This can be explained by the fact that on the low-pressure end the ice I_h-like nanocrystals present in uHDA only need to grow to become detectable, while they first have to transform to ice IX in the case of pressures ⩾0.30 GPa.

In our previous study [23] we have discussed that, in general, uHDA could show different structural remnants from its mother phase ice I_h. Besides short-range-ordered domains (i.e., nanocrystals), middle- or long-range correlations (i.e., mesoscaled structures) could also be present. However, we ruled out mesoscaled structures to be responsible for the growth of ice I_h at rather low temperatures at ⩽0.20 GPa because only nanocrystals resist the polyamorphic transformation of uHDA to low-density amorphous ice LDA. The experiments for pressures ⩾0.30 GPa presented here support the conclusion of nanocrystals being at the origin of the different crystallization behaviors of uHDA and eHDA. As discussed above, nanocrystals can transform from ice I_h to ice IX upon heating at any pressure in the range where ice IX is metastable. Indeed, our experiments provide evidence for this scenario. In contrast, the experimental findings at ⩾0.30 GPa can hardly be explained by mesoscaled structures in uHDA. These structures would have to change from ice I_h-like to ice IX-like character to reduce the onset temperature of ice IX crystallization of uHDA relative to that of eHDA—as in the case of nanocrystals. However, while it is reasonable that nanocrystals can undergo such a transition (similar to polymorphic transitions in bulk materials) [68–70], it is hard to figure out how mesoscaled correlations could do so.

Nanocrystals in uHDA might behave similarly to bulk crystals because contributions of the nanocrystals' surface to the total free energy of the system might be small due to stabilizing effects from the amorphous matrix (cf. the discussion in [68]). Bulk ice I_h can be overpressurized [71], and thus a (metastable equilibrium) phase boundary with metastable ice IX exists, as shown in water's phase diagram in

Fig. 4. That is, in the pressure range 0.1–0.2 GPa, ices I_h and IX exhibit similar free energies. The schematic free energy surface in Fig. 9 illustrates the relative stability of these two ice phases. At 0.1–0.2 GPa (left panel) ice I_h and ice IX are comparably stable, and thus ice I_h nanocrystals simply grow as uHDA is heated [23]. However, the nanocrystals are apparently subjected to a transformation upon heating at a very high pressure of 1.1 GPa (right panel) [23]. While the HDA matrix transforms to very high-density amorphous ice (VHDA) upon heating to 160 K at 1.1 GPa [52], the nanocrystals dissolve and form VHDA too [23]. Based on this observation it is reasonable to expect a correlation between the amorphous-amorphous transition on the one hand and the nanocrystal-amorphous transition on the other hand. Considering such a correlation, the nanocrystals might not transform to amorphous material at intermediate pressures (0.3–0.8 GPa) where VHDA does not form [72]. However, with increasing pressure the free energy of ice I_h increases, while the free energies of high-pressure polymorphs decrease (cf. the qualitative changes of the free energy with pressure illustrated in the left and middle panels in Fig. 9). That is, a transformation of the nanocrystals from ice I_h to, e.g., ice IX at 0.3 GPa is indeed expected. Of course, these considerations are based on the assumption that nanocrystals embedded in an amorphous matrix behave similarly to bulk crystals. Nevertheless, it has been stated above why this assumption seems to be justified.

Evidence for a similar transition of nanocrystals has also been provided in literature. So far, a polymorphic transition from a low-pressure/low-density to a high-pressure/high-density phase has been observed by Lipinska-Kalita and co-workers for a potassium-silicate glass containing β-Ga_2O_3 nanocrystals with a diameter of ∼15 nm. They studied structural changes during isothermal compression/decompression at ambient temperature by making use of energy-dispersive x-ray diffraction [68], angle-dispersive x-ray diffraction, as well as Raman scattering spectroscopy (all of them *in situ*) at pressures up to 38 GPa [69]. Starting from nanocrystals of the thermodynamically stable polymorph β-Ga_2O_3, evidence for a phase transition to α-Ga_2O_3 is found upon compression. Similar experiments on *bulk* samples of β-Ga_2O_3 (crystallites with several micrometers in diameter) done by Machon *et al.* show the same qualitative behavior as described for the nanocomposite (i.e., the transition of the low-density phase β-Ga_2O_3 to the high-density phase α-Ga_2O_3 [70]). However, in the case of the bulk material this transition is sharper than in the case of the nanocrystals being embedded in a glassy matrix. In addition to particle size effects as a potential explanation for this observation, the nanocrystals may be influenced by the glassy host matrix, thus causing differences in their phase behavior.

V. SUMMARY AND IMPLICATIONS

We have shown that in the whole pressure range of 0.10–0.50 GPa the low-temperature boundary of water's no man's land is shifted to significantly higher temperatures in studies using eHDA instead of uHDA (Fig. 1). Thus, the size of the no man's land is significantly reduced at its low-temperature side if uHDA is first transformed to VHDA which is then transformed back to eHDA. We conclude that

upon the formation of VHDA I_h-like nanocrystals present in uHDA dissolve, causing VHDA and eHDA to be more homogeneous and more stable against crystallization than uHDA. If uHDA is heated at pressures $\leqslant 0.20$ GPa, the nanocrystals simply grow, while they experience a polymorphic phase transition at pressures $\geqslant 0.30$ GPa (Fig. 3).

We want to emphasize that very recently significant progress in experiments on supercooled water was obtained by enhancing the experimental time scale at subambient pressure [34] and by extending studies at negative pressures [33,38]. In addition to these approaches, our results show that alternative routes to prepare amorphous ices exhibit large potential to increase the p-T space where supercooled water is accessible in experiments.

While we have focused on HDA here, previous studies on the crystallization behavior of two types of low-density amorphous ice (LDA$_I$ and LDA$_{II}$ [28,29,73]) at rather low pressures [23,74] await their extension to higher pressures. We expect that these two forms of LDA show a similar relation to each other with respect to the crystallization phenomenology as the two forms of HDA studied here.

A comparison of the crystallization curve $T_x(p)$ of purely amorphous LDA (i.e., LDA$_{II}$) with that of purely amorphous HDA (i.e., eHDA) has the potential to further elucidate the relation between these two states which are discussed to be connected via a first-order transition [2,30,75–77]. We note, however, that the actual locus of $T_x(p)$ is determined by an interplay of dynamics and thermodynamics.

From the perspective of dynamics, the $T_x(p)$ curves are expected to follow the glass transition curves, since the glass transition temperature T_g is a measure for the molecules' mobility, which is a factor determining crystal nucleation and growth. It has been discussed that distinct loci of $T_g(p)$ of LDA and HDA would provide strong support for the existence of two distinct liquid states of water [78,79] and, in fact, LDA and HDA indeed show distinct glass transition temperatures

at ambient pressure [7]. Hence, distinct crystallization curves $T_x(p)$ of LDA and HDA would support the existence of amorphous polymorphism in water, too. From the perspective of thermodynamics, theoretical work indicates distinct nucleation barriers for low-density and high-density water [45]. Indeed, this is confirmed by recent simulation studies on homogeneous ice nucleation in ST2 water above the liquid-liquid critical point. Analysis of the free energy cost to form a crystalline cluster reveals that its pressure dependence reflects the liquid's low- and high-density character, respectively [46]. Hence, the low-temperature proxies of the two proposed liquid states, LDA and HDA, are expected to show distinct $T_x(p)$ curves due to different energy barriers to form critical nuclei from LDA and HDA, respectively.

Moreover, since the shifted low-temperature boundary of the no man's land enables the study of HDA at significantly higher temperatures, the molecular mobility in HDA can now be probed in a much broader temperature range. In fact, evidence for the transition of HDA to a corresponding ultraviscous high-density liquid both at ambient pressure [7] and at elevated pressures [9] has been found very recently. Similarly, the now given feasibility to study HDA at higher temperatures boosts experiments aiming at a more direct investigation of the (proposed) liquid-liquid phase transition (see, e.g., the recent study on the transformation of equilibrated HDA to a low-density liquid or amorphous state [30]).

[1] O. Mishima, L. D. Calvert, and E. Whalley, Nature (London) **310**, 393 (1984).

[2] O. Mishima, L. D. Calvert, and E. Whalley, Nature (London) **314**, 76 (1985).

[3] O. Mishima and H. E. Stanley, Nature (London) **396**, 329 (1998).

[4] P. G. Debenedetti, J. Phys.: Condens. Matter **15**, R1669 (2003).

[5] J. J. Shephard, J. S. O. Evans, and C. G. Salzmann, J. Phys. Chem. Lett. **4**, 3672 (2013).

[6] T. Loerting, V. Fuentes-Landete, P. H. Handle, M. Seidl, K. Amann-Winkel, C. Gainaru, and R. Böhmer, J. Non-Cryst. Solids **407**, 423 (2015).

[7] K. Amann-Winkel, C. Gainaru, P. H. Handle, M. Seidl, H. Nelson, R. Böhmer, and T. Loerting, Proc. Natl. Acad. Sci. USA **110**, 17720 (2013).

[8] O. Mishima, J. Chem. Phys. **121**, 3161 (2004).

[9] M. Seidl, M. S. Elsaesser, K. Winkel, G. Zifferer, E. Mayer, and T. Loerting, Phys. Rev. B **83**, 100201 (2011).

[10] O. Andersson, Proc. Natl. Acad. Sci. USA **108**, 11013 (2011).

[11] P. H. Poole, F. Sciortino, U. Essmann, and H. E. Stanley, Nature (London) **360**, 324 (1992).

[12] L. Xu, P. Kumar, S. V. Buldyrev, S.-H. Chen, P. H. Poole, F. Sciortino, and H. E. Stanley, Proc. Natl. Acad. Sci. USA **102**, 16558 (2005).

[13] L. Heckmann and B. Drossel, J. Chem. Phys. **138**, 234503 (2013).

[14] F. W. Starr and F. Sciortino, Soft Matter **10**, 9413 (2014).

[15] N. Giovambattista, Adv. Chem. Phys. **152**, 113 (2013).

[16] D. T. Limmer and D. Chandler, J. Chem. Phys. **135**, 134503 (2011).

[17] D. T. Limmer and D. Chandler, J. Chem. Phys. **138**, 214504 (2013).

[18] J. C. Palmer, F. Martelli, Y. Liu, R. Car, A. Z. Panagiotopoulos, and P. G. Debenedetti, Nature (London) **510**, 385 (2014).

[19] H. Tanaka, Eur. Phys. J. E **35**, 113 (2012).

[20] V. Holten, J. C. Palmer, P. H. Poole, P. G. Debenedetti, and M. A. Anisimov, J. Chem. Phys. **140**, 104502 (2014).

[21] J. Russo and H. Tanaka, Nat. Commun. **5**, 3556 (2014).

[22] O. Mishima, J. Chem. Phys. **100**, 5910 (1994).
[23] M. Seidl, K. Amann-Winkel, P. H. Handle, G. Zifferer, and T. Loerting, Phys. Rev. B **88**, 174105 (2013).
[24] S. Klotz, G. Hamel, J. S. Loveday, R. J. Nelmes, and M. Guthrie, Z. Kristallogr. **218**, 117 (2003).
[25] C. G. Salzmann, E. Mayer, and A. Hallbrucker, Phys. Chem. Chem. Phys. **6**, 5156 (2004).
[26] C. G. Salzmann, T. Loerting, S. Klotz, P. W. Mirwald, A. Hallbrucker, and E. Mayer, Phys. Chem. Chem. Phys. **8**, 386 (2006).
[27] R. J. Nelmes, J. S. Loveday, T. Strässle, C. L. Bull, M. Guthrie, G. Hamel, and S. Klotz, Nat. Phys. **2**, 414 (2006).
[28] K. Winkel, M. S. Elsaesser, E. Mayer, and T. Loerting, J. Chem. Phys. **128**, 044510 (2008).
[29] K. Winkel, M. Bauer, E. Mayer, M. Seidl, M. S. Elsaesser, and T. Loerting, J. Phys.: Condens. Matter **20**, 494212 (2008).
[30] K. Winkel, E. Mayer, and T. Loerting, J. Phys. Chem. B **115**, 14141 (2011).
[31] P. H. Handle, M. Seidl, and T. Loerting, Phys. Rev. Lett. **108**, 225901 (2012).
[32] O. Mishima, Proc. Jpn. Acad., Ser. B **86**, 165 (2010).
[33] F. Caupin, J. Non-Cryst. Solids **407**, 441 (2015).
[34] J. A. Sellberg *et al.*, Nature (London) **510**, 381 (2014).
[35] A. Manka, H. Pathak, S. Tanimura, J. Wölk, R. Strey, and B. E. Wyslouzil, Phys. Chem. Chem. Phys. **14**, 4505 (2012).
[36] M. Chonde, M. Brindza, and V. Sadtchenko, J. Chem. Phys. **125**, 094501 (2006).
[37] A. Sepúlveda, E. Leon-Gutierrez, M. Gonzalez-Silveira, C. Rodríguez-Tinoco, M. T. Clavaguera-Mora, and J. Rodríguez-Viejo, J. Chem. Phys. **137**, 244506 (2012).
[38] G. Pallares, M. E. M. Azouzi, M. A. González, J. L. Aragones, J. L. F. Abascal, C. Valeriani, and F. Caupin, Proc. Natl. Acad. Sci. U.S.A. **111**, 7936 (2014).
[39] M. Yamada, S. Mossa, H. E. Stanley, and F. Sciortino, Phys. Rev. Lett. **88**, 195701 (2002).
[40] M. Matsumoto, S. Saito, and I. Ohmine, Nature (London) **416**, 409 (2002).
[41] E. B. Moore and V. Molinero, Nature (London) **479**, 506 (2011).
[42] D. T. Limmer and D. Chandler, Faraday Discuss. **167**, 485 (2013).
[43] F. Smallenburg, L. Filion, and F. Sciortino, Nat. Phys. **10**, 653 (2014).
[44] A thermodynamic rather than a dynamic view on this issue is provided in Refs. [45,46].
[45] R. S. Singh and B. Bagchi, J. Chem. Phys. **140**, 164503 (2014).
[46] C. R. C. Buhariwalla, R. K. Bowles, I. Saika-Voivod, F. Sciortino, and P. H. Poole, arXiv:1501.03115.
[47] S. B. Kiselev and J. F. Ely, Physica A **299**, 357 (2001).
[48] A. Cavagna, Phys. Rep. **476**, 51 (2009).
[49] E. L. Gromnitskaya, O. V. Stal'gorova, V. V. Brazhkin, and A. G. Lyapin, Phys. Rev. B **64**, 094205 (2001).
[50] O. Mishima, Nature (London) **384**, 546 (1996).
[51] I. Kohl, E. Mayer, and A. Hallbrucker, Phys. Chem. Chem. Phys. **3**, 602 (2001).
[52] T. Loerting, C. Salzmann, I. Kohl, E. Mayer, and A. Hallbrucker, Phys. Chem. Chem. Phys. **3**, 5355 (2001).
[53] Y. Suzuki and Y. Tominaga, J. Chem. Phys. **133**, 164508 (2010).

[54] G. Tammann, *Kristallisieren und Schmelzen: Ein Beitrag zur Lehre der Änderungen des Aggregatzustandes* (J. A. Barth, Leipzig, 1903).
[55] G. Tammann, Z. Anorg. Chem. **63**, 285 (1909).
[56] P. W. Bridgman, Proc. Am. Acad. Arts Sci. **47**, 441 (1912).
[57] B. Kamb, Acta Crystallogr. **17**, 1437 (1964).
[58] B. Kamb, A. Prakash, and C. Knobler, Acta Crystallogr. **22**, 706 (1967).
[59] B. Kamb and A. Prakash, Acta Crystallogr., Sect. B: Struct. Crystallogr. Cryst. Chem. **24**, 1317 (1968).
[60] S. J. La Placa, W. C. Hamilton, B. Kamb, and A. Prakash, J. Chem. Phys. **58**, 567 (1973).
[61] B. Minceva-Sukarova, W. F. Sherman, and G. R. Wilkinson, J. Phys. C: Solid State Phys. **17**, 5833 (1984).
[62] Y. P. Handa, D. D. Klug, and E. Whalley, J. Phys. Colloq. **48**, C1-435 (1987).
[63] W. B. Durham, S. H. Kirby, H. C. Heard, and L. A. Stern, J. Phys. Colloq. **48**, C1-221 (1987).
[64] W. B. Durham, S. H. Kirby, H. C. Heard, L. A. Stern, and C. O. Boro, J. Geophys. Res., [Solid Earth and Planets] **93**, 10191 (1988).
[65] C. G. Salzmann, P. G. Radaelli, J. L. Finney, and E. Mayer, Phys. Chem. Chem. Phys. **10**, 6313 (2008).
[66] D. J. Prior, S. Diebold, R. Obbard, C. Daghlian, D. L. Goldsby, W. B. Durham, and I. Baker, Scr. Mater. **66**, 69 (2012).
[67] M. Seidl, G. Zifferer, and T. Loerting (unpublished).
[68] K. E. Lipinska-Kalita, B. Chen, M. B. Kruger, Y. Ohki, J. Murowchick, and E. P. Gogol, Phys. Rev. B **68**, 035209 (2003).
[69] K. E. Lipinska-Kalita, O. A. Hemmers, P. E. Kalita, G. Mariotto, S. Gramsh, R. J. Hemley, and T. Hartmann, J. Phys. Chem. Solids **69**, 2268 (2008).
[70] D. Machon, P. F. McMillan, B. Xu, and J. Dong, Phys. Rev. B **73**, 094125 (2006).
[71] M. Bauer, K. Winkel, D. M. Toebbens, E. Mayer, and T. Loerting, J. Chem. Phys. **131**, 224514 (2009).
[72] T. Loerting, K. Winkel, M. Seidl, M. Bauer, C. Mitterdorfer, P. H. Handle, C. G. Salzmann, E. Mayer, J. L. Finney, and D. T. Bowron, Phys. Chem. Chem. Phys. **13**, 8783 (2011).
[73] K. Winkel, D. T. Bowron, T. Loerting, E. Mayer, and J. L. Finney, J. Chem. Phys. **130**, 204502 (2009).
[74] M. S. Elsaesser, K. Winkel, E. Mayer, and T. Loerting, Phys. Chem. Chem. Phys. **12**, 708 (2010).
[75] O. Mishima, K. Takemura, and K. Aoki, Science **254**, 406 (1991).
[76] M. M. Koza, H. Schober, H. E. Fischer, T. Hansen, and F. Fujara, J. Phys.: Condens. Matter **15**, 321 (2003).
[77] N. Giovambattista, K. Amann-Winkel, and T. Loerting, Adv. Chem. Phys. **152**, 139 (2013).
[78] L. Xu, S. V. Buldyrev, N. Giovambattista, C. A. Angell, and H. E. Stanley, J. Chem. Phys. **130**, 054505 (2009).
[79] N. Giovambattista, T. Loerting, B. R. Lukanov, and F. W. Starr, Sci. Rep. **2**, 390 (2012).
[80] H. Kanno, R. J. Speedy, and C. A. Angell, Science **189**, 880 (1975).
[81] P. V. Hobbs, *Ice Physics* (Clarendon, Oxford, 1974).
[82] C. G. Salzmann, P. G. Radaelli, E. Mayer, and J. L. Finney, Phys. Rev. Lett. **103**, 105701 (2009).